First-principles studies of the stability of Zintl ions in alkali-tin alloys: I. Crystalline intermetallic compounds

2001 J. Phys.: Condens. Matter 13 959

(http://iopscience.iop.org/0953-8984/13/5/314)

INSTITUTE OF PHYSICS PUBLISHING JOURNAL OF PHYSICS: CONDENSED MATTER

J. Phys.: Condens. Matter **13** (2001) 959–980 www.iop.org/Journals/cm PII: S0953-8984(01)16909-2

First-principles studies of the stability of Zintl ions in alkali–tin alloys: I. Crystalline intermetallic compounds

O Genser and J Hafner

Institut für Materialphysik and Centre for Computational Materials Science, Universität Wien, Sensengasse 8/12, A-1090 Wien, Austria

Received 5 September 2000

Abstract

The systematic variations of the crystal structure, phase stability, electronic structure and chemical bonding properties of equiatomic alkali–tin alloys as functions of the size of the alkali atom have been studied for the example of equiatomic alkali–tin alloys using *ab initio* local density calculations. It is demonstrated that the formation of the polyanionic phases of KSn and NaSn with tetrahedral Sn_4 clusters may be interpreted within the Zintl principle: the large electronegativity difference leads to an at least formally complete electron transfer from the alkali to the tin atoms and to the formation of strong covalent bonds stabilizing the Sn_4^{4-} 'Zintl ions' which are isoelectronic and isostructural to the P_4 molecule. Charge transfer is also the dominant mechanism in LiSn; however, due to the smaller size of its alkali ion, the remaining intercluster interactions are too strong, so the Sn ions form an extended network (in the form of corrugated planes) rather than isolated polyanions. The LiSn structure is also discussed from the point of view of a simple ionic model such as is realized in the CsCl structure. It is shown that the simple ionic model is destabilized by direct Sn–Sn interactions. Local density functional theory is shown to provide an accurate description of the complex crystal structures of these alloys and a rationale for the observed structural trends in alkali–group-IV alloys.

(Some figures in this article are in colour only in the electronic version; see `www.iop.org`)

1. Introduction

Alloys of alkali metals with group-IV elements display rather complex phase diagrams and peculiar variations of their structural, thermodynamic and electronic properties with composition. At the equiatomic composition, the structure of the crystalline intermetallic compounds is characterized by the formation of tetrahedral clusters of the polyvalent atoms—the most prominent example is the NaPb structure (see figure 1) which is assumed by the equiatomic alloys of Na, K, Rb and Cs with Pb and Sn [1–3]. Moreover, tetrahedra also occur in the equiatomic compounds of Na, K, Rb and Cs with Ge and Si [4, 5]. The formation of

0953-8984/01/050959+22$30.00

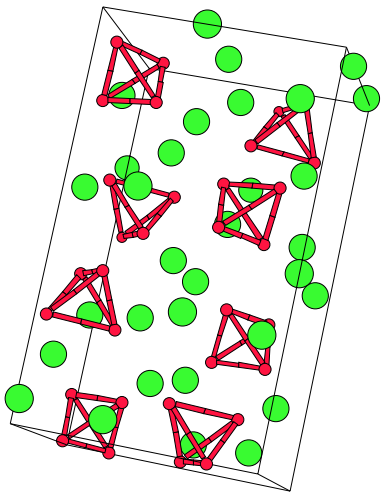

Figure 1. The elementary cell of the tetragonal NaPb structure. The tetravalent atoms forming the tetrahedral polyanions are shown as dark balls with nearest-neighbour bonds drawn as solid bars. Alkali atoms are drawn as light spheres.

the tetrahedral clusters may be interpreted in terms of a general building principle for alloys with a large difference in valence and/or electronegativity formulated in the early 1930s by Zintl and co-workers [6, 7]. The Zintl principle is most easily illustrated by considering an equiatomic alkali–tin alloy such as KSn. As a consequence of the large electronegativity difference, the single valence electron of K is transferred to the Sn atom. The resulting Sn ion is isoelectronic to P and As which form tetrahedral P_4 and As_4 molecules in the gas phase. Accordingly the Sn atoms in KSn form tetrahedral Sn_4^{4-} polyanions, separated by the K^+ cations. In this idealized picture all the valence electrons occupy Sn s and Sn p orbitals. Indeed the electronic band structure resembles closely the molecular level structure of As_4, with the Fermi level in the covalent gap between the bonding and antibonding p states of the tetrahedron [8, 9]. Note that the tetrahedral pnictide molecules are stable only in the dilute-gas phase. Likewise, a sufficiently large separation of the tetrahedral polyanions by the alkali ions is very important [10]—this explains the decreasing stability of the polyanionic phase in the sequence CsSn–RbSn–KSn–NaSn–LiSn.

The Zintl principle can be extended to a variety of other alloys. In systems with an alkali ion as the cation, due to the electron transfer, a group-III atom is isoelectronic to silicon and the anions form a diamond-type sublattice. This is indeed observed for the B32 compounds LiAl, LiGa, LiIn, NaIn and NaTl [6]. In alkali–pnictide alloys the 'polyanions' are infinite selenium-like spiral chains such as the $\{Sb^-\}_\infty$ helices in KSb [11, 12]. In alkali–chalcogenide ions the polyanions are dimers isostructural and isoelectronic to halogen molecules, with Te_2^{2-} in crystalline KTe [13] as a prominent example.

The Zintl principle is not restricted to equiatomic alloys in which a single valence electron per ion is transferred. In the alloys LiGa–Li_3Ga_2–Li_2Ga the 'polyanions' form a diamond-type sublattice like in Si, puckered layers like in crystalline As and infinite chains like in Se, corresponding to the increasing charge state of the Ga ions with increasing Li content of the alloys (although at higher Li content the bonds in the polyanions are always somewhat electron deficient) [14, 15]. In Na_2Tl, tetrahedral Tl_4^{8-} polyanions are formed which are isostructural and isoelectronic to the polyanions in the alkali–IV alloys [16]. Tetrahedral polyanions occur also in compounds such as $CaSi_2$ and $BaSi_2$ [17]—in such a case the two valence electrons provided by the alkaline-earth atom are shared among two silicon atoms. The Zintl principle can also be extended beyond binary alloys and provides a key to the understanding of the often very complex crystal structures [18].

The Zintl principle requires the formal transfer of *all* valence electrons to the more electronegative atoms. The fact that early electronic structure calculations led to the conclusion that the real charge transfer determined e.g. by the spatial integration of the charge density over atomic spheres is small has caused frequent criticism of the Zintl argument [19–21]. However, it has now become clear that spatial charge transfer (which is also notoriously difficult to quantify) is not the main point: the real distinguishing feature is that all occupied valence electron states are determined by the strong attractive electron–ion potential of the polyvalent element:

(a) In the alkali–III alloys the valence states form more or less perfect sp^3 hybrids like in the elemental semiconductors [22, 23].
(b) In the alkali–IV alloys the valence bands may be indexed according to the irreducible representations of the tetrahedron group [8, 9].
(c) In the alkali–V alloys the structure of the valence bands is determined by the splitting of the p bands into bonding, non-bonding and antibonding parts (with the Fermi level in the non-bonding–antibonding gap), in analogy to the band structure of the chalcogen elements [24, 25].

The conclusion is that if a charge-transfer compound is defined as a system in which the occupied valence bands are describable in terms of linear combinations of the atomic wavefunctions of the polyvalent species, the Zintl principle is confirmed by quantum mechanics.

Over the last two decades, interest in polyanionic bonding has been revived by the discovery that the polyanionic clusters have considerable stability and flexibility. The tetrahedral-cluster compounds NaSn and CsPb have been shown to undergo a two-stage melting process with high-temperature solid phases characterized by rapidly changing dynamical disorder [26–29]. This disorder is associated with fast reorientations of the tetrahedral polyanions coupled to a migration of the alkali cations. The high-temperature phases of both compounds are characterized by a lower crystalline symmetry than the low-temperature phases. The reduced symmetry allows accommodation of additional partly filled cation sites needed for the diffusive cation motion, but leaves the polyanionic clusters intact. In addition, there is considerable evidence from diffraction studies and other experiments that the polyanionic clusters survive in the liquid state. The alkali–Sn and alkali–Pb alloys have been investigated with particular care. Neutron and x-ray diffraction experiments [30–36] demonstrate the existence of a first sharp diffraction peak (FSDP) in the static structure factor and of a three-peak structure of the first maximum in the radial distribution function. The simultaneous presence of a FSDP and of a tripartite structure of the first coordination shell (with a maximum intensity at the composition of the crystalline polyanionic compound) have been interpreted as indications of the survival of the polyanionic species in the molten phase. The diffraction experiments have been extended to high temperatures and low densities, demonstrating the persistence of the short- and intermediate-range order even up to the highest temperatures measured [36–38]. At the concentration where the ordering is most pronounced, thermodynamic properties (e.g. the Darken excess-stability function, mixing enthalpy and heat capacity) and electronic transport show drastic deviations from ideal behaviour [39–43]. A large excess heat capacity just above the melting point scales with the stability of the polyanionic phase and decreases with increasing temperature. The electrical resistivity is in the regime of strong electron scattering (300 to 3000 $\mu\Omega$ cm) at the composition of the polyanionic phase. The temperature derivative of the resistivity is negative in the same concentration range, indicating the opening or the formation of a band gap. The decrease of the excess heat capacity and of the electrical resistivity have been interpreted in terms of a temperature-induced dissociation of the polyanions. This leads, however, to a certain

conflict with the recent temperature-dependent diffraction studies indicating a persistence of the structural anomalies at temperatures where the thermodynamic anomalies have already largely vanished.

Resistivity measurements on and photoemission spectroscopy of quench-condensed amorphous alkali–Sn films [44–46] demonstrate the semiconducting character of the amorphous alloys (high resistivity, absence of a Fermi edge), in analogy with the corresponding crystalline compounds. Similar evidence for a polyanionic local order exists also for molten alloys of alkali metals with polyvalent elements from groups III, V and VI (for recent reviews see, e.g., references [38, 47–49].

However, even diffraction studies provide only one-dimensional projections of the three-dimensional atomic arrangement and hence no unique evidence for the existence of polyanionic clusters in the liquid. Such evidence could be provided by modelling studies or computer simulations. Reverse Monte Carlo (RMC) calculations represent an attempt to reconstruct the three-dimensional atomic arrangement from the one-dimensional projections provided by the diffraction experiments [50]. RMC calculations for liquid-alkali–lead alloys have been performed by Howe and McGreevy [51] and Stolz *et al* [52]. The common conclusion is that only a small fraction of the Pb atoms form isolated tetrahedra—the majority form a rich variety of Pb conformations which can be considered as fragments of tetrahedra linked together to form a three-dimensional network. However, one has to remember that RMC solutions are not unique and tend to produce the most random structure compatible with the diffraction data.

Computer simulations for liquid-alkali–group-IV alloys have been performed at various levels of sophistication, ranging from molecular dynamics (MD) simulations based on empirical pair forces chosen to enforce the existence of Pb_4 tetrahedra [53, 54] or effective potentials derived from pseudopotential and linear screening theories [55] to *ab initio* local density functional molecular dynamics [56–62]. The *ab initio* MD simulations generally yield good agreement of the calculated structure factors with the diffraction data, but—similar to the RMC calculations—they suggest the existence of a wide variety of local conformations of the group-IV atoms embedded in an extended network, and no dominance of isolated tetrahedra. This is not so surprising for liquid Na–Sn (references [57, 60, 61]) where the phase diagram clearly indicates that the crystalline polyanionic compound NaSn has only marginal stability, but this is rather disappointing in the case of Cs–Pb (reference [59]) and K–Si (reference [56]), where the diffraction studies indicate a very high degree of local order in the melt. However, one has to remember that the *ab initio* MD simulations have been performed on rather small samples and over time intervals of only a few picoseconds (this is perhaps the more stringent restriction). Also some dependence on the initial configuration has been noted. Also it must be admitted that it remains unclear whether the crystalline polyanionic structure is stable in the local density approximation.

In this work we present an *ab initio* local density functional study of the structure, stability, chemical bonding and electronic properties of equiatomic alkali–group-IV alloys. The conditions determining the relative stability of polyanionic (i.e. NaPb-type) and ionic (i.e. CsCl-type or structurally related) phases are studied for the example of the series Li, Na, K–Sn. In the companion paper these studies will be extended to the molten phases of these alloys.

2. Methodology

Our investigations have been performed using the Vienna *ab initio* simulation package VASP [62–64], which is based on the following principles:

(1) Electronic exchange and correlation are treated in the local density approximation (LDA) [65], using the functional developed by Ceperley and Alder as parametrized by Perdew and Zunger [66].
(2) The solution of the generalized Kohn–Sham equations is performed using an efficient iterative matrix-diagonalization routine based on a sequential band-by-band residual-minimization (RMM) method [63, 67] applied to the one-electron energies. An improved Pulay mixing [68] was used to achieve self-consistency of the charge density and the potential [63].
(3) The optimization of the atomic geometry is performed via a conjugate-gradient minimization of the total energy with respect to the volume and shape of the unit cell and the internal atomic coordinates, using the analytic Hellmann–Feynman forces acting on the atoms. The structural optimization was stopped when the change in the total (free) energy between two successive steps became smaller than 10^{-3} eV.
(4) The calculations have been performed using fully non-local optimized ultrasoft pseudopotentials [69, 70]. Details of the pseudopotentials are given below.
(5) Brillouin-zone integrations were performed using a grid of Monkhorst–Pack special points [71] and the linear tetrahedron method with Blöchl corrections [72].
(6) The energies calculated as a function of volume were interpolated using a Murnaghan equation of state to determine the bulk modulus [73].

2.1. Ultrasoft pseudopotentials

Ultrasoft pseudopotentials for the alkali elements have been generated for an s^1 atomic reference configuration. For Li and Na the s and p components have been modelled with two non-local projectors (i.e. two reference energies [70]), while the d component has been described by a norm-conserving potential and a single projector. The d component of the pseudopotential has been chosen as the local potential. Cut-off radii for pseudowavefunctions and augmentation functions, together with the kinetic energies of the highest plane-wave components used in the expansion of the pseudized wavefunctions and augmentation function, are listed in table 1. For comparison, we have also generated a norm-conserving pseudopotential for Na: to achieve an accuracy comparable with that of the ultrasoft potentials, the plane-wave cut-off has to be increased from 49 eV to 165 eV. For K the d component is also modelled by an ultrasoft potential; in this case the local component of the pseudopotential is given by the all-electron potential truncated at a radius of $R_{\mathrm{loc}} = 1.71$ au. The calculated equilibrium volumes, cohesive energies and bulk moduli are compiled in table 2. These results reflect the well-known overbinding property of the LDA which is particularly notorious for the alkali metals: the errors in the calculated equilibrium atomic volumes of the bcc phase are -12.2% (Li), -11.50% (Na) and -9.8% (K); they are accompanied by an overestimate of the bulk modulus by about 15 to 20%. The overbinding trend may in many (but not all) cases be corrected by including generalized gradient corrections (GGC) [74]. For the three alkali metals considered here, the GGCs reduce the errors in the equilibrium volumes to -8.6% (Li), -2.0% (Na) and +3.7% (K) and yield almost perfect agreement of the calculated bulk moduli with experiment (but note the trend to overcorrect the LDA error for K). The GGC calculations are based on pseudopotentials recalculated using gradient corrections for the atomic reference state. The stable low-temperature phase is in all cases hexagonal close packed, with structural energy differences which are of the order of the critical temperatures for the martensitic hcp $\rightarrow$ bcc transitions [75].

Table 1. Pseudopotential data: cut-off radii $R_{cut,l}$ and $R_{aug,l}$ for wavefunctions and augmentation charges; cut-off energies E_{cut} and E_{aug} for pseudowavefunctions and augmentation functions.

			s	p	d		
Li	$R_{cut,l}$	(au)	2.32	2.32	2.11		
	$R_{aug,l}$	(au)	2.60	2.60	2.11		
	E_{cut}	(eV)					76
	E_{aug}	(eV)					152
Na	$R_{cut,l}$	(au)	2.97	2.97	2.70		
	$R_{aug,l}$	(au)	3.32	3.32	2.70		
	E_{cut}	(eV)					49
	E_{aug}	(eV)					93
K	$R_{cut,l}$	(au)	3.84	3.84	3.49		
	$R_{aug,l}$	(au)	3.84	4.30	4.30		
	E_{cut}	(eV)					71
	E_{aug}	(eV)					126
			s	p	d	f	
Sn	$R_{cut,l}$	(au)	2.65	2.65	2.65	2.96	
	$R_{aug,l}$	(au)	2.96	2.96	2.96	2.96	
	E_{cut}	(eV)					106
	E_{aug}	(eV)					168

For Sn, an ultrasoft pseudopotential has been constructed for an atomic reference configuration s^2p^2. Ultrasoft pseudopotentials with two projectors (=reference energies) have been constructed for the s and p components; d and f components have been modelled by norm-conserving potentials; the f pseudopotential has been chosen as the local potential. In the LDA, the equilibrium atomic volume is underestimated by -2.4% for α-Sn (diamond structure) and -4.9% for β-Sn (note that the experimental reference is the low-temperature volume for α-Sn, but the room-temperature volume for β-Sn). In this case the GGCs overcorrect the LDA error; the corresponding deviations from experiment are now +6.1% (α-Sn) and +3.6% (β-Sn), respectively.

These results concerning the performance of the LDA and GGA in describing the bonding properties of the alkali metals and of tin fit very well into the general trends throughout the Periodic Table [77, 78]: within each main group of elements, the performance of the LDA improves with increasing atomic number and at the same time the effect of the GGCs increases such that for the light elements the GGCs constitute an important improvement, whereas for the heavier elements the gradient terms overcorrect the LDA error. This has been demonstrated here for the alkalis, but holds also for the polyvalent main-group elements (see references [77, 78] for the pnictide and chalcogenide elements). One also notes a decrease of the LDA error when going from the left to the right of the Periodic Table, paralleled by an increasing importance of the GGCs (on adding GGCs the volume expands by 8.5% for α- and β-Sn and by about 13% for Sb and Se). One should also keep in mind that a number of studies on both metallic and insulating phases [77–79] have shown that at fixed volume, the LDA and LDA + GGC lead to almost identical structural predictions, the effect of the GGCs being limited to adding an isotropic term to the pressure. This holds in the present case for the tetragonal β-tin phase whose axial ratio is at fixed volume the same in the LDA and in the GGA. In addition we have calculated the phonon spectrum of α-tin and found that at the respective equilibrium volumes both the LDA and the GGA lead to very good agreement with

Table 2. Equilibrium atomic volume Ω (in Å^3), cohesive energy E_{coh} (in eV) and bulk modulus B (in kbar) for Li, Na and K in the bcc, fcc and hcp structures, compared with experiment. LDA and GGA refer to the results achieved with and without generalized gradient corrections.

			Ω (Å^3/atom)	E_{coh} (eV/atom)	B (kbar)
Li	LDA	bcc	18.96	−2.0379	147
		fcc	18.93	−2.0419	149
		hcp	18.94	−2.0459	150
	GGA	bcc	19.73	−1.9064	136
		fcc	19.67	−1.9101	137
		hcp	19.68	−1.9102	136
	Experiment	bcc	21.60[a]		131[c]
Na	LDA	bcc	33.29	−1.4533	91
		fcc	33.33	−1.4541	91
		hcp	33.28	−1.4587	91
	GGA	bcc	36.88	−1.3031	74
		fcc	36.87	−1.3049	75
		hcp	36.82	−1.3081	75
	Experiment	bcc	37.66[a]		76[d]
		hcp	37.81[b]		76[d]
K	LDA	bcc	64.37	−1.1710	44
		fcc	64.55	−1.1726	44
		hcp	64.59	−1.1728	44
	GGA	bcc	73.99	−1.0290	37
		fcc	74.08	−1.0297	37
		hcp	74.40	−1.0311	37
	Experiment	bcc	71.26[a]		37[e]

[a] Reference [93].
[b] Reference [16].
[c] Reference [94].
[d] Reference [95].
[e] Reference [96].

the measured frequencies. A more detailed account of the LDA (GGC) descriptions of the structure and bonding of crystalline and liquid tin has been given elsewhere [76].

We have also investigated the influence of a relaxation of the 'semicore' states (3d states in tin, 3p states for the potassium) on the ground-state predictions. In both cases the result is a modest expansion ($\leqslant$1–2%) of the equilibrium volume which does not justify the vastly increased computational effort.

Concerning the decision as to whether to perform the investigations of the binary compounds with or without the GGCs, we are confronted with a dilemma: the GGCs evidently lead to a much more accurate prediction of the equilibrium volume for the alkali metals (with a slight tendency to overcorrect in the case of K), while the LDA without GGCs predicts a more accurate equilibrium density for α-Sn. Because we expect the structural and bonding properties of the compounds to be dominated by the strong Sn–Sn interactions, the present studies have been performed in the LDA.

3. Crystal structure

The crystallographic information on the equiatomic compounds of alkali and group-IV elements is summarized in table 3. Except the lithium-based compounds, all assume polyanionic structures based on tetrahedral clusters of the polyvalent atoms. The structural variants differ mostly in the ratio of the intracluster to the shortest intercluster distance. In the simple cubic KGe structure [4] assumed by the compounds of K, Rb and Cs with Si and Ge (space group T_d^4, Pearson symbol cP64) this ratio varies between $d_{\text{inter}}/d_{\text{intra}} = 1.91$ for KGe and $d_{\text{inter}}/d_{\text{intra}} = 2.13$ for CsSi. As emphasized by Hewaidy *et al* [2], the shortest intercluster distances are larger than twice the outer ionic radii of Si^- and Ge^- estimated for sixfold coordination. The situation is different for the tetragonal NaPb structure (space group $I4_1/acd$, Pearson symbol tI64) [1] assumed by the compounds of Na, K, Rb and Cs with Sn and Pb. Here the relatively short distance between neighbouring tetrahedra ($d_{\text{inter}}/d_{\text{intra}} = 1.15, 1.27, 1.15, 1.45$ in NaPb, NaSn, KPb and KSn, respectively) indicates that at least a weak covalent interaction between the polyvalent ions must exist. In the monoclinic structures of NaSi (space group C_{2h}^6, Pearson symbol C32) and NaGe (space group C_{2h}^5, Pearson symbol mP32) [80] we find an intermediate situation with $d_{\text{inter}}/d_{\text{intra}} = 1.86$ for NaSi and 1.57 for NaGe. The differing strength of the intercluster interactions also shows up in the electronic structure. As demonstrated by Springelkamp *et al* [8] and Tegze and Hafner [9], the valence band structure of all compounds may be interpreted in terms of the eigenstates of the tetrahedron. Within an sp basis the s states reduce to the A_1 and T_2 irreducible representations, the p states to A_1, T_2, E (bonding) and T_1, T_2 (antibonding). For the KGe, NaGe and NaSi compounds, the bonding p band close to the Fermi level is clearly split into three subbands corresponding to the molecular levels A_1, T_2 (triply degenerate) and E (doubly degenerate) and containing the appropriate number of electrons [9]. In NaPb and KPb on the other hand these three states are intermixed and the bonding–antibonding gap is reduced from $E_g = 1.0$ eV in NaSi and NaGe to $E_g \sim 0.3$ eV in NaPb and NaSn.

Table 3. Crystal structures of the equiatomic alkali–group-IV alloys.

	Li	Na	K	Rb	Cs
Si	—	NaSi	KGe	KGe	KGe
Ge	LiGe	NaGe	KGe	KGe	KGe
Sn	LiSn	NaPb	NaPb	NaPb	NaPb
Pb	CsCl	NaPb	NaPb	NaPb	NaPb

A similar structural trend associated with the differences in degree of covalent bonding between the tetravalent atoms exists also for the Li-based compounds. LiPb where the Pb–Pb bonding is weak crystallizes in the CsCl structure: here the dominant feature is charge ordering, keeping the Pb ions apart. LiSn crystallizes in a monoclinic lattice (space group $P/2m$, Pearson symbol mP6) [81] which shows some structural similarity with Li–Pb phases, but also some with the structures of the pnictide elements. In LiSn the atoms form flat layers parallel to the (a, b) plane such that each atom is surrounded by four atoms of the other kind (see figure 2). In LiPb the same atomic arrangement (except for a different ratio of the edge lengths) exists in the (110) planes. However, differences exist in the stacking of these planes. Whereas in LiPb adjacent layers are shifted by half of the identity along the $[\bar{1}10]$ direction such that there are no direct Pb–Pb neighbours, the stacking sequence in the direction normal to the layer in LiSn (about [130]) is such that adjacent layers are displaced only by 1/3 of the repeat distance along the x-axis. This smaller displacement leads to direct Sn–Sn interactions in

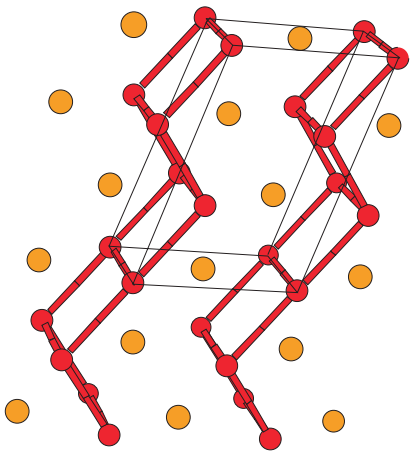

Figure 2. The crystal structure of LiSn. Sn atoms are shown as dark spheres, Li atoms as light spheres. Nearest-neighbour bonds within the corrugated layers discussed in the text are shown by bars.

neighbouring layers such that corrugated layers parallel to the (b, c) plane are formed (see figure 2). Within the corrugated planes each atom is fourfold coordinated by like atoms; in addition there are eight unlike neighbours in adjacent sheets. Altogether the difference between the LiPb and LiSn structures is caused by the stronger tendency to form bonds between the Sn atoms [2, 82].

The corrugated Sn layers in LiSn are reminiscent of the puckered atomic layers in the crystal structures of the pnictide elements and in the compound Li_3Ga_2 [14, 15]. The analysis of the electronic structure and chemical bonding has demonstrated that the Li_3Ga_2 may be interpreted within the Zintl concept, although at this composition the pnictide-like polyanionic bonds are electron deficient [14]. In LiSn the electron transfer is sufficient to make Sn^- isoelectronic to the pnictide atoms. However, according to the $(8 - N)$ rule one would expect a threefold coordination of Sn^- (in analogy to the A7 structure of the pnictide elements and to the Li_3Ga_2 structure) and not the fourfold coordination realized in the LiSn structure. A threefold coordination in the polyanionic sublattice is realized only in the LiGe lattice [83]. Hence LiSn is intermediate between the ionometallic phase LiPb and the polyanionic LiGe compound. In the following we use *ab initio* local density theory to investigate the stability of (Li, Na, K)Sn in the NaPb, LiSn and LiPb (CsCl) structures with the aim of exploring the transition from polyanionic to more conventional forms of chemical bonding.

3.1. Polyanionic cluster compounds

Within the tetragonal cell of NaPb the Pb atoms occupy sites (32g) with internal coordinates (x, y, z). Na atoms are placed on sites (16e) with coordinates $(x, 0, \frac{1}{4})$ and (16f) with coordinates $(x, \frac{1}{4} + x, \frac{1}{8})$, space group $I4_1/acd$. Hence at fixed volume the total energy must be minimized with respect to six structural parameters. Table 4 summarizes our results for the optimized crystal structures. For KSn the equilibrium volume is underestimated by -11%; the tetragonal cell is slightly elongated. The excess volume of alloying, however, is quite well described: $\Delta\Omega(\text{theor}) = -32.5\%$; $\Delta\Omega(\text{exp}) = -28.3\%$. The internal structural parameters are calculated with good accuracy. For the interatomic distances we find that the Sn–Sn intracluster distances are underestimated by -2%, but the shortest intercluster Sn–Sn distances are underestimated by -6.5%, reducing the ratio $d_{\text{inter}}/d_{\text{intra}}$ from 1.45 to 1.385. Compared to the nearest-neighbour distance between the fourfold-coordinated Sn atoms in α-Sn, the bond length between the threefold-coordinated Sn atoms in the tetrahedral polyanions

Table 4. Lattice constants a and c, internal structural parameters, atomic volume Ω, volume and heat of formation $\Delta\Omega$ and ΔH, bulk modulus B and interatomic distances d_{ij} for NaPb-type (Pearson symbol tI64) alkali–tin compounds. Experimental values are given in parentheses.

		KSn[a]	NaSn[b]	LiSn
a (Å)		10.837 (11.42)	10.132 (10.46)	9.265
c (Å)		17.963 (18.57)	17.054 (17.39)	15.728
c/a		1.658 (1.626)	1.683 (1.663)	1.698
Ω (Å^3)		32.96 (37.84)	27.35 (29.73)	21.09
$\Delta\Omega$ (%)		−32.5 (−28.3)	−18.4 (−17.2)	−19.7
ΔH (eV/atom)		−0.447	−0.248	−0.310
B (kbar)		184	219	249
A1 (16e)	x	0.865 (0.865)	0.876 (0.872)	0.876
A2 (16f)	x	0.625 (0.625)	0.626 (0.626)	0.620
Sn (32g)	x	0.066 (0.065)	0.070 (0.070)	0.082
	y	0.133 (0.137)	0.122 (0.126)	0.154
	z	0.927 (0.931)	0.938 (0.935)	0.934
$d_{\text{intra}}^{\text{Sn-Sn}}$ (Å)	$1x$ $(2x)$[c]	2.91 (2.96)	2.96 (2.97)	3.02
	$2x$ $(1x)$	2.92 (2.98)	2.98 (2.97)	3.08
$d_{\text{inter}}^{\text{Sn-Sn}}$ (Å)	$1x$	4.03 (4.31)	3.57 (3.76)	3.15
$d^{\text{A-A}}$ (Å)	$2x$	3.74 (3.86)	3.54 (3.61)	3.11
	$2x$	3.83 (4.03)	3.54 (3.57)	3.40
	$1x$	3.72 (4.04)	3.61 (3.72)	3.27
$d^{\text{A-Sn}}$(Å)	Minimum[d]	3.51 (3.67)	3.25 (3.35)	2.90
	Maximum[d]	3.66 (3.84)	3.47 (3.53)	3.25

[a] Experimental data after reference [2].
[b] Experimental data after reference [15].
[c] Frequency of nearest-neighbour bonds per site.
[d] Minimum and maximum distances in nearest-neighbour alkali–Sn pairs.

is increased from 2.785 Å to 2.91–2.92 Å (both LDA values). The alkali atoms surround the polyanions in the form of a distorted tetrahedron such that each K_4Sn_4 group forms a distorted cube. The shortest K–K distances are, at 3.74 Å, considerably compressed compared to the interatomic distance in the pure alkali metal ($d_1(\text{K}) = 4.37$ Å in the LDA). Compared to experiment, the LDA error in the K–K distances varies between −3.7% and −7.9%; for the K–Sn distances the error varies between −4 and −5%. Altogether the analysis of the optimized LDA crystal structure shows that the LDA allows for a larger compression of the K–K distances than found experimentally, and this also leads to reduced distances of the polyanionic units from each other.

These conclusions are corroborated by the analysis of the optimized NaSn structure: the LDA error in the lattice constants is smaller than in KSn; the volume of formation is predicted quite accurately. However, as in KSn, the calculated ratio of intercluster to intracluster distances is reduced to $d_{\text{inter}}/d_{\text{intra}} = 1.206$ compared to an experimental value of 1.266. The Sn–Sn distances within the tetrahedra are predicted to be slightly larger than in KSn (by 0.05 Å), while according to experiment the bond lengths are the same. The Na–Na nearest-neighbour distances are slightly underestimated (but now only by −1.9% to −3.5%). In contrast to the case for KSn, the shortest Na–Na distances in NaSn are not compressed compared to the pure metal—this holds for the LDA prediction as well as for experiment.

In a hypothetical LiSn compound with the NaPb structure the polyanionic structure is clearly destabilized: the average intracluster distance of 3.06 Å is now almost equal to the shortest intercluster distance of 3.08 Å, the difference being smaller than that between the short and long bonds in the distorted Sn_4 tetrahedra. The shortest Li–Li distances are now of the same order as the Sn–Sn nearest-neighbour distances. The shortest distances are now found in Li–Sn pairs, emphasizing the trend towards a more conventional form of ionic bonding.

3.2. LiSn-type compounds

The optimized crystallographic data for the (Li, Na, K)Sn compounds in the monoclinic LiSn structure (space group $P2/m$) are compiled in table 5. At fixed volume the total energy has to be minimized with respect of the axial ratios (b/a) and (c/a), the monoclinic angle β and the internal coordinates of the A1 positions (A = Li, Na, Sn with site symmetry $2n$ $(x, 0.5, z)$) and Sn2 (sites $(2m)$ $(x, 0, z)$). For the stable LiSn compound, the equilibrium atomic volume is slightly underestimated by -5.8%, but the excess volume, axial ratios and monoclinic angle are in good agreement with experiment. The coordinates of the Li1 and Sn2 sites are predicted quite accurately (those of the Li2 and Sn1 atoms lying in the (a, b) plane are fixed by symmetry). Altogether the LDA leads to an accurate description of the arrangement of both Li and Sn atoms on corrugated planes parallel to the (b, c) plane. Compared to pure Sn in the diamond structure and to the tetrahedral clusters in the polyanionic compounds, the average Sn–Sn bond length is slightly elongated ($d_{\mathrm{dia}}^{\mathrm{Sn-Sn}} = 2.79$ Å, $d_{\mathrm{tetra}}^{\mathrm{Sn-Sn}} \simeq 3.02$ Å, $d_{\mathrm{Li-Sn}}^{\mathrm{Sn-Sn}} = 2.95$–3.16 Å, all calculated in the LDA), reflecting a reduced strength of the covalent Sn–Sn bond, in accordance with the increasing Sn–Sn coordination number (in the LiSn structure each atom has eight unlike and four like neighbours at approximately equal distances). The shortest Li–Li distances are larger than the distances in body-centred cubic Li ($d_{\mathrm{bcc}}^{\mathrm{Li-Li}} = 2.91$ Å), in spite of the expected electron transfer from Li to Sn and the small diameter of the Li^+ ion. This suggests that direct Li–Li bonding plays only a minor role. On the other hand the Li–Sn distances are smaller than the average Li–Li and Sn–Sn distances, emphasizing the importance of heteronuclear bonding and of electrostatic effects.

For the hypothetical NaSn and KSn compounds with the LiSn structure, the calculations predict an increasing distortion of the lattice resulting from the increasing size of the alkali atom (see table 5): the monoclinic cell is elongated along the a-axis; the internal coordinates of the Sn2 atoms change in such a way that not only does the distance between the corrugated Sn layers decrease, but in addition the layers are flattened (cf. figure 2). The internal coordinates of the Na2 and K2 sites on the other hand are only weakly affected; the alkali–alkali distances show only a modest increase on replacing Li by Na and K. This means that while the Li–Li distances are almost the same as in pure bcc Li ($d^{\mathrm{Li-Li}} = 2.91$ Å), the K–K bonds are strongly compressed ($d^{\mathrm{K-K}} = 4.37$ Å). The flattening of the Sn layers is a consequence of the fact that the strong Sn–Sn bonds cannot be too much strained on expansion of the lattice. The flattening of the corrugated Sn layers also means that the K2 atoms do not protrude as deeply into the Sn layers as the Li2 atoms (see figure 2); the alkali–tin bond lengths increase and are now larger than the average like-atom bond lengths, so the electrostatic energy becomes less favourable, and this adds to the destabilizing effect of the strained covalent Sn–Sn bonds.

The LiSn structure with its fourfold-coordinated Sn atoms is rather unexpected from the point of view of the Zintl concept. As, assuming complete charge transfer, the Sn atoms carry a formal negative charge and are isoelectronic to the group-V elements, the formation of a three-connected network common to the heavier pnictide elements (As, Sb, Bi) is expected. Very recently, the stability of different four-connected networks (planar, zigzag and stairs as in the LiSn case) has been discussed by Hoffmann and co-workers [87] on the basis of

Table 5. Lattice parameters (a, b, c, β), internal structural parameters[a], atomic volume Ω, volume and heat of formation $\Delta\Omega$ and ΔH, bulk modulus B and interatomic distances d^{i-j} in LiSn-type (Pearson symbol mP6) alkali–tin compounds. Experimental values are given in parentheses (reference [81]).

		LiSn	NaSn	KSn
a (Å)		5.041 (5.17)	5.692	6.460
b (Å)		3.160 (3.18)	3.272	3.345
c (Å)		7.505 (7.74)	8.012	8.148
b/a		0.627 (0.615)	0.575	0.517
c/a		1.489 (1.497)	1.408	1.261
β (Å)		104.8 (104.5)	103.4	102.6
Ω (Å^3)		19.26 (20.53)	24.19	28.64
$\Delta\Omega$ (%)		−26.7 (−26.4)	−27.9	−41.4
ΔH (eV/atom)		−0.399	−0.233	−0.214
B (kbar)		409	328	225
A1 ($2n$)[a]	x	0.270 (0.263)	0.298	0.322
	z	0.328 (0.336)	0.330	0.337
Sn2 ($2m$)	x	0.240 (0.234)	0.190	0.155
	z	0.662 (0.660)	0661	0.662
$d^{\mathrm{Sn-Sn}}$ (Å)	$1x$ (—)[b]	2.95 (3.00)	2.96	2.95
	$1x$ ($2x$)	3.08 (3.16)	3.14	3.13
	$2x$ ($2x$)	3.16 (3.18)	3.27	3.35
$d^{\mathrm{A-A}}$ (Å)[a]	$1x$ (—)	2.95 (3.00)	2.96	2.95
	$1x$ ($2x$)	3.08 (3.16)	3.14	3.13
	$2x$ ($2x$)	3.16 (3.18)	3.27	3.35
$d^{\mathrm{A-Sn}}$ (Å)[a]	Minimum[c]	2.92 (3.01)	3.24	3.49
	Maximum[c]	3.03 (3.09)	3.33	3.77

[a] A = Li, Na, K.
[b] Frequency of nearest-neighbour bonds.
[c] Minimum and maximum of the alkali–tin pair nearest-neighbour distances.

extended Hückel theory. It was pointed out that there are large differences in bond strength of isoelectronic compounds of Sn, Sb and Te arising from different degrees of admixture of antibonding interactions with the highest occupied valence states—at a constant valence electron concentration, the antibonding character is larger for Sn than for Sb or Te. This can be further tracked back to a greater s, p mixing in Sn which is due to the more extended character of the Sn valence orbitals. In addition it was concluded that the Li ions have a larger influence on the structure, not only because of their small size, but also by influencing the effective electron count on the Sn sites.

3.3. CsCl-type compounds

Finally we have considered also compounds with a hypothetical CsCl structure. Here every atom is surrounded by eight unlike neighbours; like atoms are only next-nearest neighbours, so the formation of direct covalent bonds between the polyvalent species is suppressed and the bonding is essentially ionic. The results compiled in table 6 demonstrate that the structure

Table 6. Lattice constant a, atomic volume Ω, volume and heat of formation $\Delta\Omega$ and ΔH, bulk modulus B and nearest- and next-nearest-neighbour distances for alkali–tin compounds with a Cs–Cl structure.

	LiSn	NaSn	KSn
a (Å)	3.354	3.630	3.960
Ω (Å^3)	18.87	23.93	31.05
$\Delta\Omega$ (%)	−27.7	−28.1	−36.4
ΔH (eV/atom)	−0.380	−0.156	−0.009
B (kbar)	429	329	227
$d^{\mathrm{A-Sn}}$ (Å)	2.905	3.144	3.429
$d^{\mathrm{Sn-Sn,A-A}}$ (Å)	3.354	3.630	3.960

is less favourable than either the LiSn and NaPb structures. However, for LiSn the structural energy difference is only ΔE(LiSn–CsCl) = 0.019 eV/atom ($\simeq$220 K). For the heavier compounds the structural energy differences increase rapidly; for CsCl-type Li, K–Sn the heat of formation is essentially zero.

3.4. Phase stability

Table 7 compares the calculated heats and volumes of formation of (Li, Na, K)Sn in the three crystal structures considered in each case. While for the polyanionic compounds the heat of formation increases with increasing alkali/Sn size ratio, it decreases for the alloys with the LiSn or CsCl structure. This can be attributed to the increasing strength of the covalent intracluster bonds with an increasing separation of the clusters on one hand, and to a decreasing electrostatic energy with increasing lattice distortion resulting from an increasing size ratio on the other hand. For all compounds we find a strong contraction on alloying which increases with increasing size (i.e. also increasing compressibility) of the alkali atom and is distinctly smaller for the polyanionic phase. It has been shown [84, 85] that the volume of formation of binary simple metal alloys may be estimated quite successfully from low-order perturbation theory in terms of the balance between the change in the electron-gas energy and the elastic energy necessary to expand and compress the individual atomic spheres. For the (Li, Na, K)Sn alloys, the low-order estimate yields $\Delta\Omega = -20, -30.5$ and -44% respectively, in reasonable agreement with the exact LDA results for the LiSn structure. For the polyanionic compounds the actual compression (both in LDA and experiment) is much smaller. This agrees with conclusions from the analysis of a wide class of covalent compounds and may be attributed to the stiffness of the strong covalent bonds.

Table 7. Volume and heat of formation of alkali–tin compounds in the NaPb, LiSn and CsCl structures (stable phases are underlined).

		LiSn	NaSn	KSn
$\Delta\Omega$ (%)	NaPb	−19.7	<u>−18.4</u>	<u>−32.5</u>
	LiSn	<u>−26.7</u>	−27.9	−41.4
	CsCl	−27.7	−28.1	−36.4
ΔH (eV/atom)	NaPb	−0.310	<u>−0.321</u>	<u>−0.447</u>
	LiSn	<u>−0.399</u>	−0.233	−0.214
	CsCl	−0.380	−0.156	−0.009

4. Electronic structure and chemical bonding

In this section we discuss the phase stability and chemical bonding in relation to the electronic spectrum.

4.1. Electronic structure of polyanionic phases

Figure 3 shows the total electronic densities of states of the three alloys in the NaPb structure, figure 4 shows the angular-momentum-decomposed local densities of states for KSn and figure 5 the electron dispersion relations along the main symmetry directions. The DOSs display a common pattern: the lowest groups of bands with binding energies ranging between about -10 eV and -5 eV are Sn s bands derived from the molecular orbitals of the Sn_4 tetrahedra belonging to the $\Gamma_1(A_1)$ and $T_4(T_2)$ irreducible representations of the tetrahedral $\bar{4}32m$ (T_d) point group. These bands contain exactly one electron per formula unit or two electrons per Sn atom. The bands around the Fermi level show intensity at both the alkali and Sn sites (the partial DOSs have been calculated by projecting each plane-wave component of an eigenstate onto spherical waves within atomic spheres; see Eichler *et al* [86] for details). Integration over atomic spheres shows that local charge neutrality is quite well preserved (although the exact numbers depend on the choice of the alkali and Sn radii, which is not unique). However, this is not the main result: we find that the DOS on the Sn sites has almost

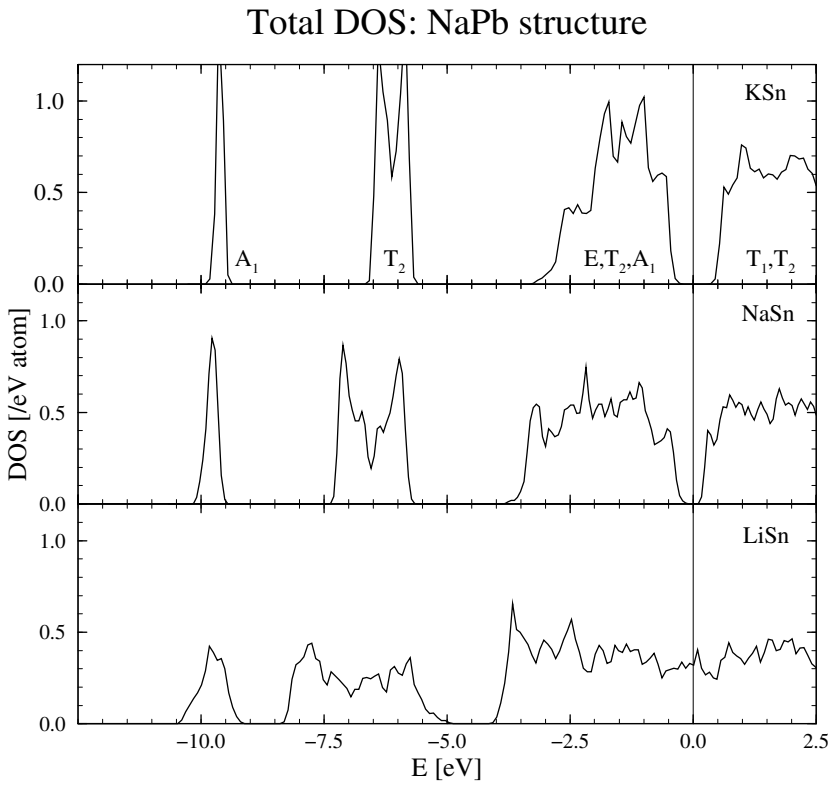

Figure 3. Total electronic densities of states of (K, Na, Li)Sn in the NaPb structure. For the KSn compound, the main peaks are labelled according to the irreducible representations of the tetrahedron group T_d (cf. the text).

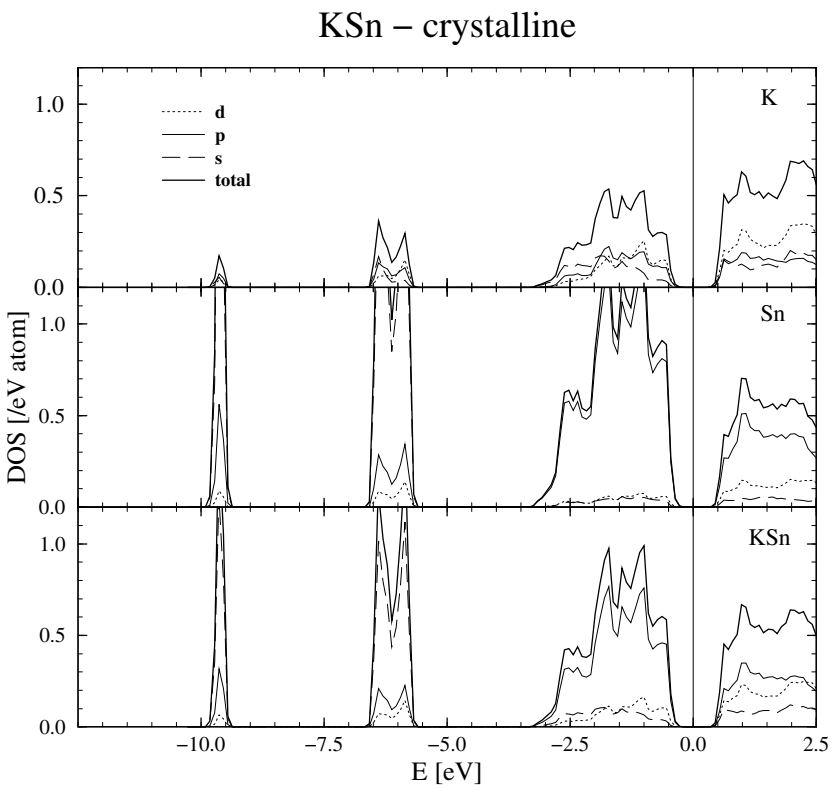

Figure 4. Angular-momentum-decomposed partial electronic densities of states on K and Sn sites in the polyanionic KSn compound.

pure Sn p character, whereas the DOS on the alkali sites has strongly mixed s, p, d character. This suggests that the local alkali DOS results mainly from the overlap of the Sn p states into the neighbouring alkali spheres, and that the valence and conduction bands close to the Fermi level may be interpreted in terms of linear combinations of Sn p states with tetrahedral symmetry belonging to the $\Gamma_1(A_1)$, $\Gamma_3(E)$, $2*\Gamma_4(T_2)$ and $\Gamma_5(T_1)$ irreducible representations. They split into the bonding combinations E, T_2, A_1 and antibonding combinations T_1 and T_2 (cf. figures 3 and 4); the Fermi level falls into the bonding–antibonding gap. In the solid the molecular eigenstates of the Sn_4 tetrahedra are broadened into bands due to the interaction among adjacent tetrahedra. This is particularly evident from the electronic dispersion relations shown in figure 5. The point-group symmetry of the Sn_4 tetrahedra determines also the structure of the Sn s bands which decompose into two subbands containing 0.5 and 1.5 electrons per Sn atom and is derived from the A_1 and T_2 irreducible representations. Again the dispersion relations shown in figure 5 illustrate the effect of the intertetrahedral interactions.

Both KSn and NaSn are predicted to be narrow-gap semiconductors with a direct gap of 0.6 eV at Γ. Hence the electronic band structure conforms very well with that expected from the Zintl picture. In the series KSn–NaSn–LiSn we find an increasing tendency to broadening of the band due to an increasing interaction among adjacent tetrahedra, scaling with a decreasing $d_{\mathrm{inter}}^{\mathrm{Sn-Sn}}/d_{\mathrm{intra}}^{\mathrm{Sn-Sn}}$ ratio (cf. table 3).

Our results are in reasonably good agreement with those obtained by Springelkamp *et al* [8] for NaSn using the augmented-spherical-wave method. The homologous compounds KPb and

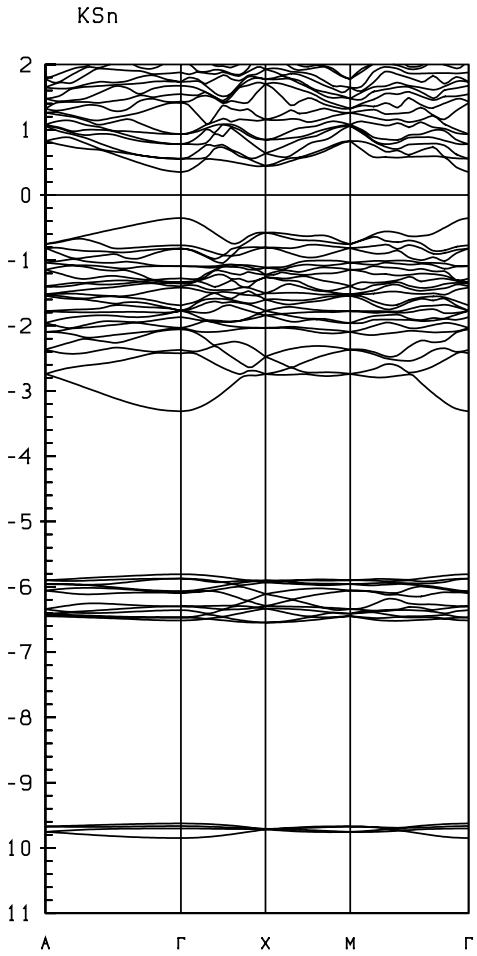

Figure 5. Electronic dispersion relations along the main symmetry directions in KSn.

NaPb have been studied by Tegze and Hafner [9] using the linear muffin-tin orbital (LMTO) method. The main characteristics of the electronic spectrum are very similar for the Pb and Sn compounds; the main differences consist in a larger s–p splitting in the alkali–lead compounds resulting from relativistic effects which tend to lower the s states relative to the p states, and a more pronounced separation in the Sn-based compounds between the s bands derived from the A_1 and T_2 molecular orbitals and between the bonding (A_1, T_2, E) and antibonding (T_1, T_2) p bands, reflecting a stronger covalent interaction. The semiconducting gap at the Fermi level is reduced to about 0.3 eV in the Pb compounds.

Although they do not crystallize in the NaPb structure, the polyanionic germanides and silicides of the heavier alkalis and NaGe and NaSi (for a discussion of their crystal structures see the preceding section) show similar electronic structure and bonding properties, albeit with an even more pronounced covalent character: the semiconducting gap increases from 0.3 eV in (Na, K)Pb to about 0.6 eV in (Na, K)Sn and KGe and to 1.0 eV in NaGe and NaSi (LMTO calculations of reference [9]); the splitting of the bonding part of the valence band into A_1, T_2, E subbands becomes more pronounced. All of this is a direct consequence of the increasing intercluster separation; cf. the discussion in section 3.

However, the formation of a semiconducting gap requires not only a sufficiently large bonding–antibonding splitting in the Sn p band; in addition the lowest alkali states must be pushed above the Fermi level. In this respect it is important that not only do the alkali ions separate the Sn_4^{4-} clusters, but also the polyanions isolate the alkali ions from each other. Actually, the alkali ions occupy positions in front of the triangular faces of the tetrahedra (cf. figure 1). This creates a substantial repulsive electrostatic potential at the alkali sites contributing to the shift of the eigenvalues. A shift of the alkali ions from these positions leads to an alkali-dominated bond with a large dispersion crossing the Fermi level. However, due to the strong chemical compression on alloying, the shortest Na–Na distances in NaSn are still comparable to those in pure sodium metal, while in KSn the shortest K–K distance is even 15% shorter than in bcc potassium (LDA and experiment). This leads to an appreciable K contribution of strong 3d character to the lowest conduction band, which counterbalances the increasing bonding–antibonding splitting, so the width of the gap is just the same in KSn as in NaSn.

4.2. Polyanionic bonding

It has been pointed out, not only for the Zintl polyanions, but even for the pnictide molecules [88] that the p-electron bonding in tetrahedral clusters should not be considered as a conventional two-electron–two-centre covalent bond. Hart *et al* [88] have suggested that in the P_4 molecule electron-density maxima are found above the three triangular tetrahedron faces, arising from the overlap of three p lobes stretching from each P site along the edges of a cube on which four opposite corners are occupied by the P atoms (see figure 6). Such a picture would also explain the position of the alkali ions attracted by the accumulation of negative charge and the large overlap of the Sn p states into the alkali spheres. This conjecture is examined here in terms of the electron-density distribution of the Sn p bands in KSn (see figure 7). The electron density plotted in this figure is obtained by integrating over the energy range from -3.7 eV up to the top of the valence band. The equidensity contours demonstrate that the electrons in these bands are concentrated around the Sn_4 tetrahedra confirming the Zintl picture. However, the electron distribution does not conform with the picture proposed by Hart *et al*: the p lobes do not protrude in the direction of the alkali sites, but are rather oriented along the edges of the tetrahedra, following a local rehybridization of the p states. This leads to an enforced intracluster bonding and a reduced Sn–alkali bonding.

Figure 6. A sketch of the electron-density distribution postulated for the P_4 molecule (after Hart *et al* [88]).

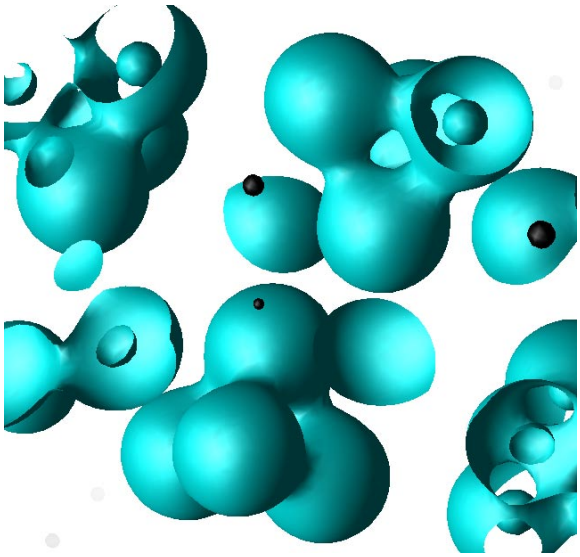

Figure 7. Isodensity surfaces of the electron density of the bonding Sn p band in KSn. Note that the density is centred around the Sn sites and along the Sn–Sn bonds. At the edges of the elementary cell the isodensity surfaces are cut open, showing the Sn ions inside. The black spheres represent the alkali atoms.

4.3. Electronic structure of LiSn-type compounds

The total electronic densities of states of LiSn, NaSn and KSn in the LiSn and CsCl structures are shown in figure 8; the angular-momentum-decomposed local DOSs are shown only for LiSn in figure 9. Again the valence band splits into an Sn s band at higher binding energy and an Sn p band around the Fermi level. The alkali atoms make only a very small contribution to the lower Sn s band; their contribution to the Sn p band has mixed s–p character (but with more weight on the p states) for the lighter alkalis and shows an increasing d admixture for the heavier elements. In LiSn and NaSn the s- and p-band complexes overlap; in KSn we find a gap of nearly 2 eV between the s and p bands. All three LiSn-type compounds are metallic, with a DOS at E_F which increases slightly in the sequence LiSn–NaSn–KSn. The s, p mixing evident from the partial electronic DOS hence confirms the extended Hückel analysis of Hoffmann and co-workers [87] discussed in connection with the structural phase stability. The more metallic character of the hypothetical LiSn-type KSn compound is a consequence of the narrowing of the Sn p band arising from the increased average Sn–Sn distances (see table 5).

The electronic spectrum of the hypothetical CsCl-type compounds is not too different from that of the LiSn-type phases; see figure 8. Here too the Li states play a minor role. The s, p splitting is more pronounced; an internal gap opens already for NaSn. The total density of states is essentially that of a simple cubic metal such as As, Sb, Bi under elevated pressure [89–91]—this is another illustration of the Zintl principle. In simple cubic As, Sb and Bi the exactly half-filled band makes the simple cubic lattice unstable against a Peierls distortion leading to the trigonal A7 structure [92]. Hence one would expect LiSn to assume a threefold-coordinated structure such as is realized in the LiGe structure [83] or in Li_3Ga_2 [15], with the Sn ions occupying positions on an As-like sublattice, and form a gap or pseudogap in the middle of the Sn p band. However, LiSn is intermediate between LiPb, which assumes an undistorted CsCl lattice, and LiGe, where the formation of three strong covalent Ge–Ge bonds

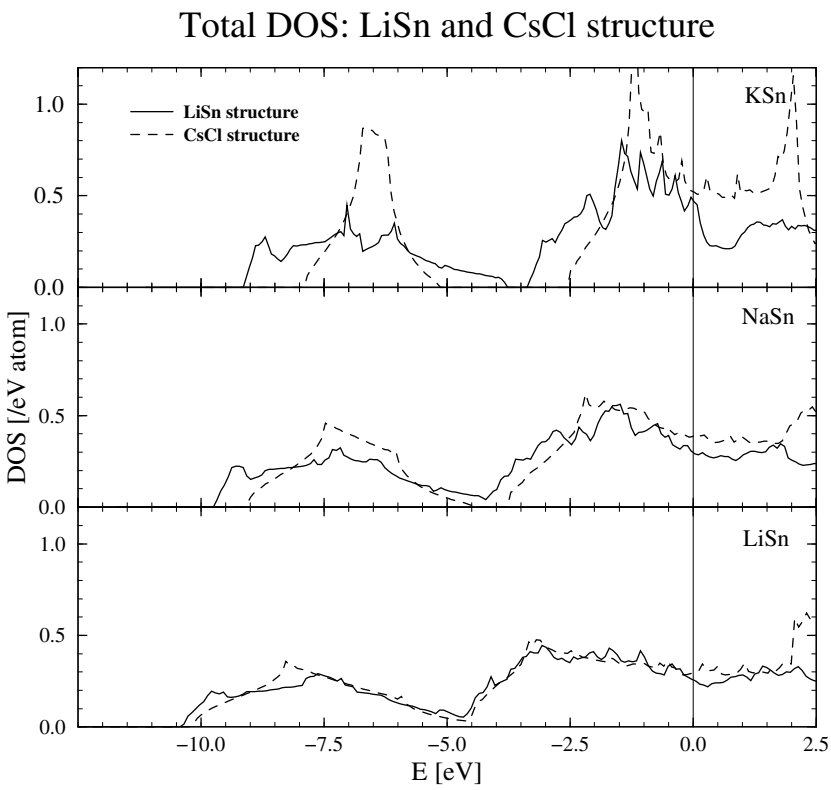

Figure 8. Total electronic densities of states of LiSn, NaSn and KSn in the LiSn structure (full lines) and in the CsCl structure (broken lines). The energy scales are matched at the Fermi level.

leads to the formation of an As-like sublattice. In LiSn the Sn–Sn interactions are just strong enough to break the strong chemical short-range order of the CsCl lattice and to establish some direct Sn–Sn contacts. Heterocoordination (each atom in LiSn is surrounded by eight unlike and four like neighbours at about equal distances; see table 4) and electrostatic interactions determine the electronic structure and chemical bonding.

5. Conclusions

We have presented a comprehensive analysis of the structural and electronic properties of equiatomic alkali–tin alloys within the local density approximation. We find that the trend from essentially ionic bonding in compounds of the lightest alkali metal (Li) with the heaviest group-IV element (Pb) to polyanionic bonding dominated by strong covalent bonds within the polyanionic clusters and weaker ionic interactions between the polyanions and the alkali cations with increasing size of the alkali and increasing electronegativity of the group-IV element is well described by the local density approximation. The *ab initio* total-energy calculations presented here are restricted to the series LiSn–NaSn–KSn, but the results are well in line with earlier electronic structure results for a broader series of I–IV alloys (although the earlier studies were restricted to calculations of the electronic structure and did not touch the structural problem). Here we show that the polytetrahedral structures with nearly undistorted Sn_4^{4-} tetrahedra are stable for KSn and NaSn and that the stability depends strongly on the

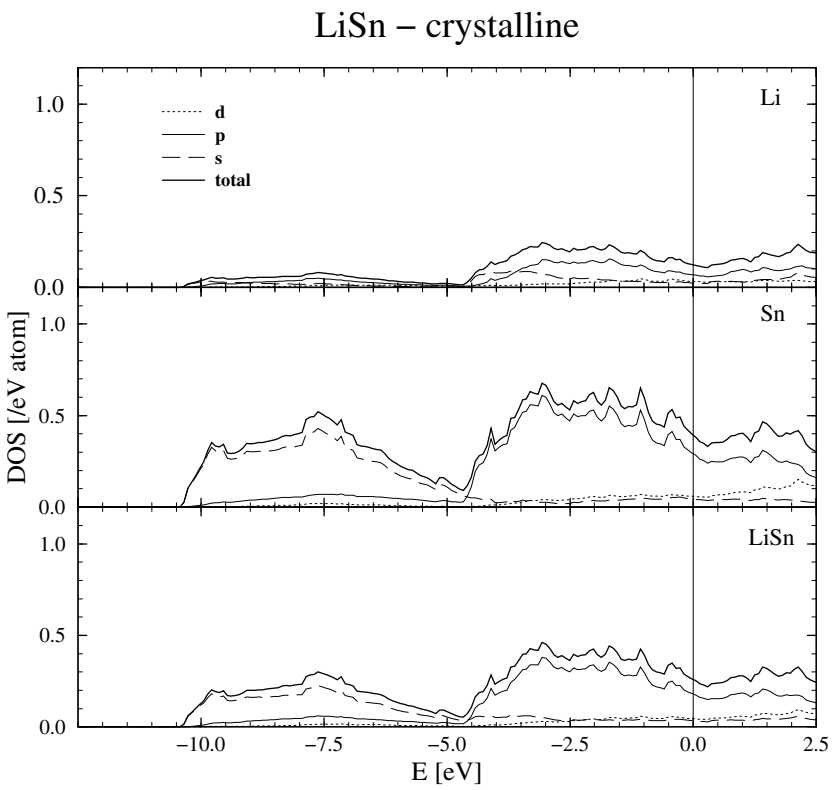

Figure 9. Angular-momentum-decomposed electronic local densities of states in LiSn.

size ratio—the size of the alkali atom being important for isolating the polyanions from each other and preventing the formation of intercluster bonds. In LiSn the size of the alkali ions is evidently insufficient and a structure with an extended corrugated planar Sn network is preferred. The monoclinic LiSn structure is only marginally more stable than the CsCl lattice, which is formed when the ionic character of the band becomes dominant.

We have also presented a detailed analysis of the electronic spectrum. In particular we find that the polyanionic compounds NaSn and KSn are narrow-gap semiconductors (with a bonding–antibonding Sn p gap) while the more ionic LiSn-type and CsCl-type compounds are predicted to be metallic. While the site-projected integrated densities of states would seem to suggest that charge transfer is small, the analysis of the angular-momentum-decomposed DOS and of the electron densities demonstrates that the Zintl picture describes the physics correctly—the non-vanishing alkali DOS is merely a consequence of the rather extended character of the molecular orbitals of the Sn_4^{4-} polyanion and of their overlap into the alkali spheres. In the companion paper these studies are extended to the liquid phase for all three compounds.

Acknowledgments

This work was supported by the Austrian Science Funds under projects No P10445-PHYS and P11353-PHYS and by the Austrian Ministry for Science through the Centre for Computational Materials Science.

References

[1] Marsh R E and Shoemaker D P 1953 *Acta Crystallogr.* **6** 197
[2] Hewaidy I F, Busmann E and Klemm W 1964 *Z. Anorg. Allg. Chem.* **328** 283
[3] Müller W and Volk K 1977 *Z. Naturf.* b **32** 709
[4] Busmann E 1961 *Z. Anorg. Allg. Chem.* **313** 90
[5] Witte J and von Schnering H G 1964 *Z. Anorg. Allg. Chem.* **327** 260
[6] Zintl E and Brauer G 1933 *Z. Phys. Chem.* B **20** 245
[7] Zintl E and Wolterdorf G 1935 *Z. Elektrochem.* **41** 876
[8] Springelkamp F, de Groot R A, Geertsma W, van der Lugt W and Mueller F M 1985 *Phys. Rev.* B **32** 2319
[9] Tegze M and Hafner J 1989 *Phys. Rev.* B **39** 8263
Tegze M and Hafner J 1989 *Phys. Rev.* B **40** 9841
[10] Geertsma W, Dijkstra J and van der Lugt W 1984 *J. Phys. F: Met. Phys.* **14** 1833
[11] Busmann E and Lohmeyer S 1961 *Z. Anorg. Allg. Chem.* **312** 53
[12] von Schnering H G, Hönle W and Krogull G 1979 *Z. Naturf.* b **34** 1678
[13] Böttcher P 1988 *Angew. Chem. Int. Edn Engl.* **27** 759
[14] Hafner J and Jank W 1991 *Phys. Rev.* B **44** 11 662
[15] Müller W and Stöhr J 1977 *Z. Naturf.* b **32** 631
[16] Hansen D A and Smith J F 1967 *Acta Crystallogr.* **22** 836
[17] Schäfer H, Janzon K H and Weiss A 1963 *Angew. Chem.* **75** 451
[18] Nesper R, von Schnering H G and Curda J 1986 *Chem. Ber.* **119** 3576
[19] Zunger A 1978 *Phys. Rev.* B **17** 2582
[20] Asada T, Jarlborg T and Freeman A 1981 *Phys. Rev.* B **24** 510
Asada T, Jarlborg T and Freeman A 1981 *Phys. Rev.* B **24** 875
[21] Pis Diez R, Iniguez M P, Alonso J A and Aramburu J A 1995 *J. Mol. Struct. (Theochem)* **330** 267
[22] Hafner J and Weber W 1985 *Phys. Rev.* B **33** 747
[23] Christensen N E 1985 *Phys. Rev.* B **32** 207
[24] Tegze M and Hafner J 1992 *J. Phys.: Condens. Matter* **3** 2449
[25] Seifert-Lorenz K and Hafner J 1999 *Phys. Rev.* B **59** 829
Seifert-Lorenz K and Hafner J 1999 *Phys. Rev.* B **59** 843
[26] Price D L, Saboungi M L, Reijers H T J, Kearley G and White R 1991 *Phys. Rev. Lett.* **66** 1894
[27] Price D L and Saboungi M L 1991 *Phys. Rev.* B **44** 7289
[28] Saboungi M L, Fortner J, Howells W S and Price D L 1993 *Nature* **365** 237
[29] Price D L, Saboungi M L and Howells W S 1995 *Phys. Rev.* B **51** 14 923
[30] Alblas B P, van der Lugt W, Dijkstra J, Geertsma W and van Dijk C 1983 *J. Phys. F: Met. Phys.* **13** 2465
[31] Reijers H R J, van der Lugt W and van Dijk C 1987 *Physica* B **144** 404
[32] Takeda S, Harada S, Tamaki S, Matsubara E and Waseda Y 1987 *J. Phys. Soc. Japan* **56** 3936
[33] Saboungi M L, Bromqvist R, Volin K J and Price D L 1987 *J. Chem. Phys.* **87** 2278
[34] Reijers H R J, van der Lugt W, van Dijk C and Saboungi M L 1989 *J. Phys.: Condens. Matter* **1** 5229
[35] Reijers H R J, Saboungi M L, Price D L, Richardson J W, Volin K J and van der Lugt W 1989 *Phys. Rev.* B **40** 6018
[36] Reijers H T J, Saboungi M L, Price D L and van der Lugt W 1990 *Phys. Rev.* B **41** 5661
[37] Stolz M, Leichtweiß O, Winter R, Saboungi M L, Fortner J and Howells W S 1994 *Europhys. Lett.* **27** 221
[38] Winter R 1997 *Thermodynamics of Alloy Formation* ed Y A Chang and F Sommer (London: The Minerals, Metals and Materials Society) p 143
[39] Tamaki S, Ishiguro T and Takeda S 1982 *J. Phys. F: Met. Phys.* **12** 1613
[40] Saboungi M L, Reijers H T J, Blander M and Johnson G K 1988 *J. Chem. Phys.* **89** 5869
[41] Geertsma W and Saboungi M L 1995 *J. Phys.: Condens. Matter* **7** 4803
[42] van der Marel C, van Oosten A B, Geertsma W, and van der Lugt W 1982 *J. Phys. F: Met. Phys.* **12** 2349
[43] van der Lugt W and Geertsma W 1987 *Can. J. Phys.* **65** 326
[44] Avci R and Flynn C P 1979 *Phys. Rev.* B **19** 5967
[45] Gremaud A *et al* 2001 *Helv. Phys. Acta* at press
[46] Madel O 1999 *Doctoral Thesis* TU Chemnitz
[47] Saboungi M L, Geertsma W and Price D L 1990 *Annu. Rev. Phys. Chem.* **41** 207
[48] van der Lugt W 1996 *J. Phys.: Condens. Matter* **8** 6115
[49] Hafner J, Seifert-Lorenz K and Genser O 2001 *J. Non-Cryst. Solids* at press
[50] McGreevy R L and Pusztai L 1988 *Mol. Simul.* **1** 359
[51] Howe M A and McGreevy R L 1991 *J. Phys.: Condens. Matter* **3** 577

[52] Stolz M, Winter R, Howells W S and McGreevy R L 1995 *J. Phys.: Condens. Matter* **7** 5733
[53] Toukan K, Reijers H T J, Loong C K, Price D L and Saboungi M L 1990 *Phys. Rev.* B **41** 11
[54] Reijers H R J, van der Lugt W and Saboungi M L 1990 *Phys. Rev.* B **42** 3395
[55] Hafner J 1989 *J. Phys.: Condens. Matter* **1** 1133
[56] Galli G and Parrinello M 1991 *J. Chem. Phys.* **95** 7504
[57] Seifert G, Pastore G and Car R 1992 *J. Phys.: Condens. Matter* **4** L179
[58] de Wijs G A, Pastore G, Selloni A and van der Lugt W 1994 *Europhys. Lett.* **27** 667
de Wijs G A, Pastore G, Selloni A and van der Lugt W 1995 *J. Chem. Phys.* **103** 5031
[59] de Wijs G A, Pastore G, Selloni A and van der Lugt W 1993 *Phys. Rev.* B **48** 13 459
[60] Schöne M, Kaschner R and Seifert G 1995 *J. Phys.: Condens. Matter* **7** L19
[61] Seifert G, Kaschner R, Schöne M and Pastore G 1998 *J. Phys.: Condens. Matter* **10** 1175
[62] Kresse G and Hafner J 1993 *Phys. Rev.* B **48** 13 115
Kresse G and Hafner J 1994 *Phys. Rev.* B **49** 14 251
[63] Kresse G and Furthmüller J 1996 *Comput. Mater. Sci.* **6** 15
Kresse G and Furthmüller J 1996 *Phys. Rev.* B **54** 11 196
[64] Hafner J and Kresse G 1997 *Properties of Complex Inorganic Compounds* ed A Gonis, A Meike and P E A Turchi (New York: Plenum) p 69
[65] Kohn W and Sham L J 1965 *Phys. Rev.* A **140** 1133
[66] Perdew J and Zunger A 1981 *Phys. Rev.* B **23** 5048
[67] Wood D M and Zunger A 1985 *J. Phys. A: Math. Gen.* **18** 1343
[68] Pulay P 1980 *Chem. Phys. Lett.* **73** 393
[69] Vanderbilt D 1990 *Phys. Rev.* B **41** 7892
[70] Kresse G and Hafner J 1994 *J. Phys.: Condens. Matter* **6** 8245
[71] Monkhorst H J and Pack J D 1976 *Phys. Rev.* B **40** 5188
[72] Blöchl P, Jepsen O and Andersen O K 1994 *Phys. Rev.* B **49** 16 223
[73] Wallace D C 1972 *Thermodynamics of Crystals* (New York: Wiley)
[74] Perdew J P and Wang Y 1992 *Phys. Rev.* B **45** 13244
Perdew J P, Chevary J A, Vosko S H, Jackson K A, Pederson M R, Singh D J and Fiolhais C 1992 *Phys. Rev.* B **46** 6671
[75] Berliner R, Fajeu O, Smith H G and Herman R L H 1989 *Phys. Rev.* B **40** 12 086
[76] Genser O and Hafner J 2001 to be published
[77] Kresse G, Furthmüller J and Hafner J 1994 *Phys. Rev.* B **50** 13 181
[78] Seifert K, Hafner J, Furthmüller J and Kresse G 1995 *J. Phys.: Condens. Matter* **7** 3683
[79] Demuth Th, Jeanvoine Y, Hafner J and Àngyàn J 1999 *J. Phys.: Condens. Matter* **11** 3833
[80] Witte J and von Schnering H G 1964 *Z. Anorg. Allg. Chem.* **327** 260
[81] Müller W and Schäfer H 1973 *Z. Naturf.* b **28** 246
[82] Zalkin A and Ramsey W J 1958 *J. Phys. Chem.* **62** 689
[83] Menges E, Hopf V, Schäfer H and Weiss A 1969 *Z. Naturf.* b **24** 1351
[84] Hafner J 1985 *J. Phys. F: Met. Phys.* **15** L43
[85] Hafner J 1989 *The Structures of Binary Compounds* ed F R de Boer and D G Pettifor (Amsterdam: North-Holland) p 205
[86] Eichler A, Hafner J, Furthmüller J and Kresse G 1996 *Surf. Sci.* **346** 300
[87] Ienco A, Hoffmann R and Papoian G 2001 to be published
See also Papoian G and Hoffmann R 2000 *Angew. Chem. Int. Edn Engl.* **39** 2408
[88] Hart R R, Robin M B and Kubler N A 1965 *J. Chem. Phys.* **42** 3631
[89] Mattheis L F, Hamann D R and Weber W 1986 *Phys. Rev.* B **34** 2190
[90] Needs R J, Martin R M and Nielsen O H 1986 *Phys. Rev.* B **33** 3778
Needs R J, Martin R M and Nielsen O H 1987 *Phys. Rev.* B **35** 9851
[91] Sasaki T, Shindo K and Niizeki K 1988 *Solid State Commun.* **67** 569
[92] Littlewood P B 1983 *Crit. Rev. Solid State Mater. Sci.* **11** 283
[93] Pearson W B 1972 *The Crystal Physics and Chemistry of Metals and Alloys* (New York: Wiley)
[94] Day J P and Ruoff A L 1974 *Phys. Status Solidi* a **25** 205
[95] Martinson R M 1969 *Phys. Rev.* B **178** 902
[96] Smith P A and Smith C G 1965 *J. Phys. Chem. Solids* **26** 279